






## Evidence of half-integer Shapiro steps originated from nonsinusoidal current phase relation in a short ballistic InAs nanowire Josephson junction

Kento Ueda <sup>1,\*</sup> Sadashige Matsuo <sup>2,3,†</sup> Hiroshi Kamata <sup>4</sup> Yosuke Sato,<sup>1</sup> Yuusuke Takeshige <sup>1</sup> Kan Li,<sup>5</sup>  
Lars Samuelson,<sup>6</sup> Hongqi Xu <sup>5,6,7,‡</sup> and Seigo Tarucha<sup>3,§</sup>

<sup>1</sup>Department of Applied Physics, University of Tokyo, 7-3-1 Hongo, Bunkyo-ku, Tokyo 113-8656, Japan

<sup>2</sup>JST, PRESTO, 4-1-8 Honcho, Kawaguchi, Saitama 332-0012, Japan

<sup>3</sup>Center for Emergent Matter Science, RIKEN, 2-1 Hirosawa, Wako-shi, Saitama 351-0198, Japan

<sup>4</sup>Laboratoire de Physique de l'École Normale Supérieure, ENS, PSL Research University, CNRS, Sorbonne Université, Université Paris Diderot, Sorbonne Paris Cité, 24 rue Lhomond, 75231 Paris Cedex 05, France

<sup>5</sup>Beijing Key Laboratory of Quantum Devices, Key Laboratory for the Physics and Chemistry of Nanodevices, and Department of Electronics, Peking University, Beijing 100871, China

<sup>6</sup>Division of Solid State Physics and NanoLund, Lund University, Box 118, 221 00 Lund, Sweden

<sup>7</sup>Beijing Academy of Quantum Information Sciences, Beijing 100193, China



(Received 29 April 2020; revised 8 August 2020; accepted 11 August 2020; published 17 September 2020)

We report on half-integer Shapiro steps observed in a gate-tunable short ballistic InAs nanowire Josephson junction. We observed the Shapiro steps of the short ballistic InAs nanowire Josephson junction and found the half-integer steps in addition to the conventional integer steps. In this Josephson junction device the junction transmission can be varied with gate voltage. From measurements of the gate voltage and temperature dependences of the Shapiro steps, the origin of half-integer steps is assigned to the skewness of the current phase relation in the short ballistic Josephson junctions. These results will contribute to establish and control the superconductivity physics in the short ballistic semiconductor nanowires.

DOI: [10.1103/PhysRevResearch.2.033435](https://doi.org/10.1103/PhysRevResearch.2.033435)

### I. INTRODUCTION

The AC Josephson effect has long been studied as a manifestation of macroscopic quantum interference [1] as well as for application in the quantum voltage standard [2] and more recently development of superconducting qubits [3,4]. The Shapiro voltage step, as given by  $V = nhf/2e$  ( $n = 1, 2, 3, \dots$ ), is an immediate consequence of the AC Josephson effect in the presence of microwave excitation [5], reflecting the phase-mediated binding of the microwave field and the Josephson current. Therefore, the Shapiro step measurement features the current phase relation (CPR) of the junctions. The CPR is usually sinusoidal with  $2\pi$  periodicity, which produces only the integer steps in overdamped Josephson junctions [6,7]. Otherwise, anomalies appear in the Shapiro steps. For example, the fractional steps have been experimentally observed [8–14] and theoretically studied [15–17] since the 1960s. There are some different origins of half-integer steps and one of the origins is the skewness of the CPR. Since the 2000s, the fractional steps have also

been observed in the Josephson junctions whose skewness of the CPR can be controlled by some parameters. In the case of superconductor (SC)-ferromagnet-SC junctions, the CPR holds huge higher-order components only in the vicinity of the  $0-\pi$  transition temperature or thickness and the half-integer steps appear only in the vicinity [18–20]. Experimental studies on such controllable junctions are available to elucidate the origin of the half-integer steps. On the other hand, odd-integer multiples of the Shapiro steps are absent in the  $4\pi$  periodic CPR, which is observed in topological superconductors hosting Majorana fermions [21–24]. The topological features of the SC junctions have been attracting intense research interest because of their applicability to topological quantum computation [25–27]; however, the physics of the bound states remains elusive.

Josephson junctions of semiconductor nanowires can show both anomalies in the Shapiro responses. A strong magnetic field invokes the topological transition, resulting in the disappearance of the odd Shapiro steps [21]. Furthermore, when the Josephson junctions of the semiconductor nanowires are ballistic but not topological, the CPR is highly skewed [28,29]; the fractional steps are expected, although they have not yet been observed experimentally. Studies on the Shapiro steps in ballistic nanowire Josephson junctions can provide important insights into the Andreev bound-state dynamics in clean nanowire-SC junctions and may contribute to the understanding of the Josephson effect in ballistic topological junctions on semiconductor nanowires.

Here we report the observation of half-integer Shapiro steps in a gate-tunable InAs nanowire Josephson junction.

\*kento.ueda@riken.jp

†sadashige.matsuo@riken.jp

‡hqxu@pku.edu.cn

§tarucha@riken.jp

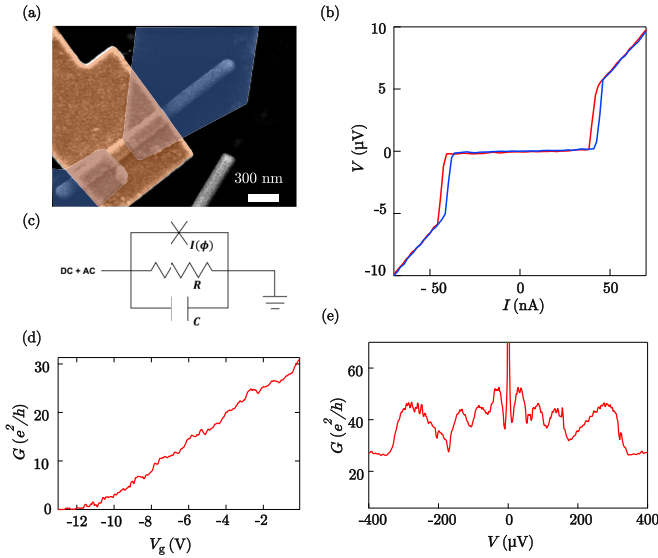


FIG. 1. (a) A SEM image of an InAs nanowire Josephson junction with a top gate electrode (orange region). This device is different from the one used in this study. The junction length between two Al electrodes (blue region) is approximately 100 nm. (b) The  $I$ - $V$  curves for our Josephson junction at  $V_g = 0$  V and  $T = 50$  mK. The red (blue) line represents the downward (upward) current sweep. (c) Diagram of an RCSJ circuit. The DC and AC are applied to the Josephson junction in parallel with the resistance and capacitance. (d) Plot of  $G$  against  $V_g$  at  $V = 1$   $\mu$ V and  $T = 4$  K. The pinch-off voltage is  $V_g = -12$  V. (e) Plot of  $G$  vs  $V$  at  $V_g = 0$  V and  $T = 50$  mK. Multiple Andreev reflections are observed.

We observed the half-integer voltage steps at  $(n/2)(hf/2e)$  ( $n = 1, 2, 3, \dots$ ). We control the junction transmission by the gate voltage of the nanowire and conclude that the half-integer steps are assigned to the skewness of the CPR appearing in the short ballistic Josephson junctions. Our numerical calculation for the short ballistic junction CPR reproduces the half-integer steps and agrees closely with the experiments, including the temperature and gate voltage dependences of the half-integer steps.

## II. JOSEPHSON JUNCTION DEVICE ON THE InAs NANOWIRE

A Josephson junction is fabricated on a self-assembled InAs single nanowire, which is placed on a Si substrate. A scanning electron microscopy (SEM) image of the fabricated device is shown in Fig. 1(a). These nanowires grown by chemical beam epitaxy have an 80-nm diameter. We transferred them on a Si substrate covered by a 285-nm-thick  $\text{SiO}_2$  film. We chose one of the nanowires and made the SC contacts of Al (60 nm) (shown in blue) on the nanowire with Ti (1 nm) as the sticking layer, resulting in the junction length between the two SCs of approximately 100 nm. We removed the native surface oxidized layer by  $(\text{NH}_4)_2\text{S}_x$  solution before the evaporation of the metals. Then the top gate electrode (orange) of Ti/Au (5 nm/150 nm) was fabricated, following atomic layer deposition of 20-nm-thick  $\text{Al}_2\text{O}_3$  [30–33]. We note that the device used in the measurement is similar but not identical to that in the figure because we were concerned

about any possible damage to our experimental device caused by the SEM observation.

## III. EXPERIMENTAL RESULTS

### A. Fundamental device properties

We first performed a DC measurement on the device. The voltage  $V$  as a function of the bias current  $I$  at a top gate voltage of  $V_g = 0$  V and temperature of  $T = 50$  mK is shown in Fig. 1(b). The red (blue) curve was obtained when  $I$  was swept in the downward (upward) direction. The supercurrent flows through the nanowire at  $V_g = 0$  V. The switching current  $I_{\text{sw}}$  and the retrapping current  $I_r$  are 40 and 38 nA, respectively.

For the quantitative analysis, we introduced a resistively and capacitively shunted junction (RCSJ) model [34,35]. The equivalent circuit for this model is shown in Fig. 1(c); we used it to study the dynamics of the phase difference between two SCs by solving

$$\frac{\hbar C}{2e} \frac{d^2 \phi}{dt^2} + \frac{\hbar}{2eR} \frac{d\phi}{dt} + I(\phi) = I_{\text{DC}} + I_{\text{AC}} \sin(2\pi ft), \quad (1)$$

where  $C$ ,  $R$ ,  $\phi$ ,  $I(\phi)$ ,  $I_{\text{DC}}$  ( $I_{\text{AC}}$ ), and  $f$  are the junction capacitance, the resistance, the phase difference between two SCs, the CPR, the applied DC (AC), and the applied frequency, respectively. This equation is transformed into a dimensionless equation with  $t' = [(2eI_{\text{sw}}R)/\hbar]t$  described as

$$\beta \frac{d^2 \phi}{dt'^2} + \frac{d\phi}{dt'} + i(\phi) = i_{\text{DC}} + i_{\text{AC}} \sin(2\pi f' t'). \quad (2)$$

Here we define  $\beta = 2eI_{\text{sw}}R^2C/\hbar$  as the Stewart-McCumber parameter [34,35] and  $f' = f/2eI_{\text{sw}}R$ . The  $\beta$  value of 0.008 was estimated from the geometry of the junction, with  $C = 130$  fF,  $R = 800$   $\Omega$  at  $V_g = 0$  V, and  $I_{\text{sw}} = 40.7$  nA. Here we used the geometric capacitance as  $C$ . Including the intrinsic capacitance [36] in the capacitance evaluation has little effect on the numerical results or our consideration discussed below. The small value of  $\beta$  means that the junction is highly overdamped. We note that there is a small difference between  $I_{\text{sw}}$  and  $I_r$  in Fig. 1(b). This can be assigned to phase instability in a capacitively and resistively shunted Josephson junction or simply due to the heating effect [37,38]. In our device, the junction is overdamped, so the hysteresis is probably assigned to the heating effect.

The differential conductance  $G$  as a function of  $V_g$  is shown in Fig. 1(d) for  $T = 4$  K, which is larger than the Al critical temperature. The pinch-off voltage depleting the carrier density of the nanowire is  $V_g = -12$  V.

We investigated  $G$  vs  $V$  at  $V_g = 0$  V and  $T = 50$  mK as shown in Fig. 1(e). We observed several conductance peaks attributed to the multiple Andreev reflections. Peaks are expected to appear at  $V = 2\Delta/en$  ( $n = 1, 2, 3, \dots$ ) with  $\Delta = 140$   $\mu$ eV of the Al superconducting gap energy. Indeed, the observed peaks are located at these voltages for  $n = 1$ –4. Observation of the multiple Andreev reflections up to the fourth order implies that elastic Andreev reflections occur sequentially at both interfaces of the Al and the nanowire. Therefore, we assumed that the interfaces are transparent enough and the nanowire between the interfaces is clean enough to enable ballistic transport through the Al-nanowire-Al junction at  $V_g = 0$  V [39].

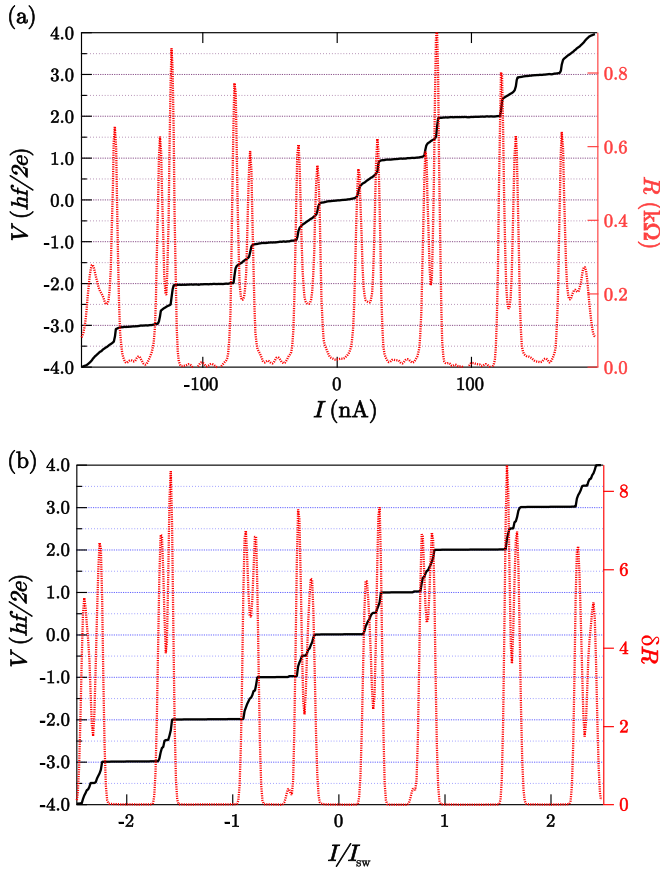


FIG. 2. (a) Shapiro steps under microwave irradiation at  $f = 4.2$  GHz,  $V_g = 0$  V, and  $P = 6$  dBm (black curve). Both conventional Shapiro steps and half-integer steps are observed. The red curve represents  $R$  of the  $I$ - $V$  curve. (b) Numerical simulated Shapiro response at  $\beta = 0.008$ ,  $f' = 0.095$ , and  $i_{AC} = 2$ . The half-integer steps are reproduced.

### B. Observed half-integer Shapiro steps

Next we applied microwave radiation to study the Shapiro response. The black curve in Fig. 2(a) represents the  $I$ - $V$  curve at  $V_g = 0$  V and  $T = 50$  mK measured for a microwave input with applied power  $P = 6$  dBm and  $f = 4.2$  GHz. The conventional Shapiro steps are observed at  $V = nhf/2e$  ( $n = 1, 2, 3, \dots$ ). Furthermore, there are additional plateaus at the half-integer multiples of  $hf/2e$ . The half-integer steps are detected at various microwave frequencies (see the Appendix). Here  $R$  as a function of  $I$  becomes zero at the integer steps as shown by the red dotted line in Fig. 2(a). The half-integer steps appear as the dips.

To determine the cause of the half-integer steps, we introduced the CPR for a short ballistic Josephson junction having a single channel which is given by

$$I(\phi) = \frac{e\Delta(T)}{2\hbar} \frac{\tau \sin(\phi)}{[1 - \tau \sin^2(\phi/2)]^{1/2}} \times \tanh\left(\frac{\Delta(T)}{2k_B T} [1 - \tau \sin^2(\phi/2)]^{1/2}\right), \quad (3)$$

where  $\Delta$ ,  $\tau$ , and  $T$  are the superconducting gap, transmission of the junction, and temperature, respectively [40–43]. This

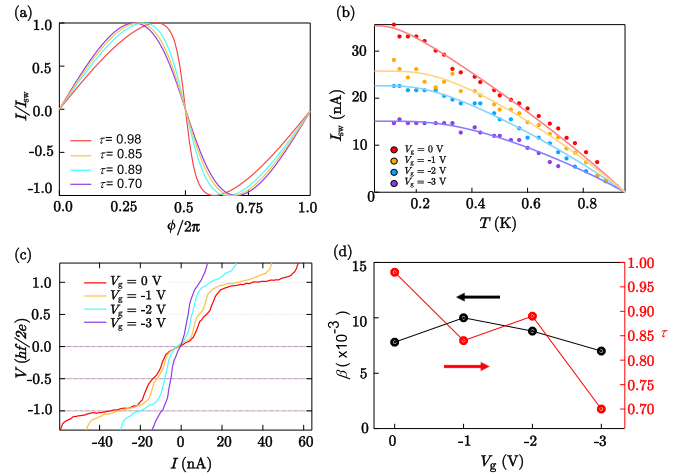


FIG. 3. (a) Comparison of short ballistic CPR curves for  $\tau = 0.98$  (red),  $\tau = 0.85$  (orange),  $\tau = 0.89$  (blue), and  $\tau = 0.7$  (purple) at  $T = 50$  mK. (b) Plot of  $I_{sw}$  vs  $T$ . The red, orange, blue, and purple dots correspond to  $V_g = 0, -1, -2,$  and  $-3$  V, respectively. These data were fit using the short ballistic CPR (see the Appendix). (c) Plot of  $I$ - $V$  curves at  $V_g = 0, -1, -2,$  and  $-3$  V with  $P = -17$  dBm and  $f = 1.8$  GHz. (d) Plot of  $\beta$  and  $\tau$  vs  $V_g$ . Here  $\tau$  decreases whereas  $\beta$  is nearly constant with decreasing  $V_g$ .

CPR is skewed from the sinusoidal function of  $\phi$  for the conventional Josephson junctions. The CPR with  $\tau = 0.98$  and  $T = 50$  mK is represented by the red line in Fig. 3(a) as the normalized supercurrent vs  $\phi$ . As previously predicted, the skewed CPR can generate the steps at the fractional quantized voltages because the skewed CPR includes higher harmonic components whose periodicity is fractions of  $2\pi$ .

We numerically calculated the Shapiro responses using the CPR with  $\tau = 0.98$  and  $T = 50$  mK in the RCSJ model. In Fig. 2(b) a typical result is shown of the calculated Shapiro steps for  $f = 4.2$  GHz,  $\beta = 0.008$ , and  $I_{sw} = 40$  nA. The black solid and red dotted lines represent  $V$  vs  $I/I_{sw}$  and the differential resistance  $\delta R$  vs  $I/I_{sw}$ , respectively. It is clear that the experimentally observed half-integer Shapiro steps are reproduced by the numerical calculation. In addition, we recognize weak features of additional steps with heights of one-third and two-thirds of the quantized voltages in the calculation. However, in the experiment we observed neither of them [see Fig. 2(a)], but the half-integer plateaus were largely tilted. We therefore suspect that the one-third and two-third steps were smeared in the experiment because of the insufficient resolution of our measurement setup. In our numerical calculation, we assumed all the channels have the same  $\tau$  for simplicity. Even with this rough assumption, the experimental results are explained well by the CPR skewness as shown in the following discussion.

### C. Gate voltage dependence of the half-integer Shapiro steps

The CPR skewness depends on  $\tau$  and  $T$ . Therefore, we investigated the  $V_g$  and  $T$  dependence of  $I_{sw}$ . From the temperature dependence of  $I_{sw}$ , we can evaluate  $\tau$  because  $I_{sw}$  is derived as the maximum of the CPR in Eq. (3). We note that the recent analytical method enables us to evaluate the

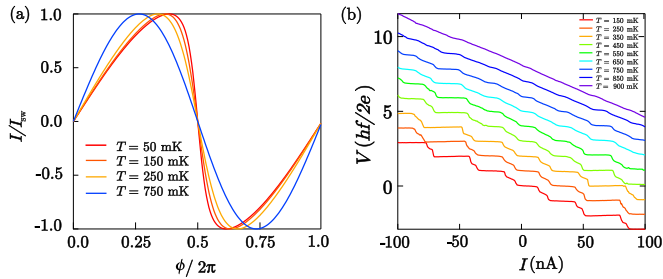


FIG. 4. (a) Comparison of short ballistic CPR curves for  $T = 50$  mK (red),  $T = 150$  mK (orange),  $T = 250$  mK (yellow), and  $T = 750$  mK (blue) at  $\tau = 0.98$ . Here  $I_{sw}$  is the simulated critical current at each temperature for  $\tau = 0.98$ . (b) Temperature dependence of the Shapiro steps at  $P = 11$  dBm and  $f = 4.2$  GHz. The y axis shows the data for 150 mK; the other data are incremented upward by  $hf/2e$ .

transmissions for each conduction channel but this method is available only for junctions with a few conduction channels [44]. Here our junction includes around 15 spin-degenerated channels, so we used the single transmission  $\tau$  as a representative. Then we measured the temperature dependence of  $I_{sw}$  at  $V_g = 0, -1, -2,$  and  $-3$  V as shown by the red, yellow, blue, and purple circles in Fig. 3(b), respectively. We carried out the numerical fitting of the experimental results with the maximum of Eq. (3) with  $\tau$  and the effective channel number as free fitting parameters. The calculated result is shown as the solid lines in Fig. 3(b). We obtained excellent fitting of the solid lines to the experimental results for  $V_g = 0, -1, -2,$  and  $-3$  V with  $\tau$  of 0.98, 0.85, 0.89, and 0.7, respectively, as shown in Fig. 3(b). The transmission tends to be smaller as the conductance decreases by the gating. In particular,  $\tau = 0.98$  for  $V_g = 0$  V is nearly unity, indicating nearly perfect transmission. The CPR or normalized supercurrent vs  $\phi$  with  $\tau = 0.98, 0.85, 0.89, 0.7$  at  $T = 50$  mK is represented in Fig. 3(a). The results indicate that the CPR skewness is remarkable at  $V_g = 0$  V because of the high transmission.

The  $V_g$  dependence of the Shapiro steps measured for  $f = 1.8$  GHz,  $P = -17$  dBm, and  $T = 50$  mK is shown in Fig. 3(c). The half-integer steps vanish before the integer steps do with decreasing  $V_g$ . First we checked  $\beta$  vs  $V_g$  because the junction dynamics in the RCSJ model highly depends on  $\beta$ . The obtained  $\beta$  vs  $V_g$  is shown in Fig. 3(d). Here  $\beta$  is as small as 0.008–0.01 in the  $V_g$  range of our measurement, indicating that the RCSJ circuit is highly overdamped. Thus, the measured  $V_g$  dependence of the half-integer steps cannot be attributed to the change in  $\beta$ . On the other hand, as shown in Fig. 3(a), the CPR skewness fades away or  $\tau$  decreases as  $V_g$  decreases. Therefore, the disappearance of the half-integer steps with decreasing  $V_g$  is attributed to the change in CPR skewness.

#### D. Temperature dependence of the half-integer Shapiro steps

Finally, to confirm the relation between the CPR skewness on the half-integer steps, we investigated the temperature dependence of the Shapiro steps at  $V_g = 0$  V. The calculated CPR with  $\tau = 0.98$  at  $T = 50, 150, 250,$  and  $750$  mK is shown in Fig. 4(a). As  $T$  increases, the CPR becomes closer to a sinusoidal function and the skewness disappears. The

$I$ - $V$  curves including the Shapiro steps measured at various temperatures between  $T = 150$  and  $900$  mK are shown in Fig. 4(b). Both the conventional integer and half-integer steps become gradually more vague as  $T$  increases. In addition, the half-integer steps almost vanish at  $T = 750$  mK, whereas the conventional steps are still visible at the even higher  $T$ . This behavior is consistent with the temperature dependence expected from the CPR as shown in Fig. 4(a). Consequently, we conclude that the observed half-integer steps originate from the skewed CPR.

## IV. DISCUSSION

We note that the observed half-integer steps are not related to the  $0$ - $\pi$  transition of the junction, which also generates half-integer steps as reported in previous research [18–20]. The  $0$ - $\pi$  transition can be invoked in a Josephson junction with the time-reversal symmetry broken [45,46] or the quantum-dot Josephson junctions [47–50]. We detected the fractional steps in the time-reversal invariant system, that is, our junction does not contain ferromagnetic materials and we applied no magnetic field. In addition, quantum dots are not formed in our nanowire as confirmed from the conductance as a function of  $V_g$ . Therefore, we can rule out these scenarios.

In addition, we discuss the nonadiabatic effect which can also produce the half-integer steps [10,11,14]. This nonadiabatic effect plays important roles in the case of  $f > 2E_{Th}/h$  in the diffusive junctions ( $E_{Th}$  is Thouless energy). The characteristic energy can be replaced by  $I_{sw}R$  in the ballistic junctions. In our experiments, the half-integer steps were observed in  $f = 1.8$  GHz at  $V_g = 0$  V as seen in Fig. 3(c) with  $I_{sw}R = 33 \mu\text{eV}$ , resulting in  $f \ll I_{sw}R$ . In addition, thermal energy at  $T = 50$  mK  $\sim 4.3 \mu\text{eV}$  is also sufficiently smaller than  $I_{sw}R$ . Furthermore, the  $V_g$  dependence of the half-integer Shapiro steps in Fig. 3(c) shows that the half-integer steps disappear at more negative  $V_g$ , although  $I_{sw}R$  at  $V_g = -3$  V decreases to  $16 \mu\text{eV}$ . If the nonadiabatic effect were the case, this smaller  $I_{sw}R$  would produce more explicit half-integer steps. Therefore, the observed half-integer steps cannot be assigned to the nonadiabatic effect.

## V. CONCLUSION

We have observed half-integer Shapiro steps in the short ballistic Josephson junction of an InAs nanowire. We associated this observation with the skewed CPR in a short ballistic Josephson junction by using numerical calculations. This association was further supported by the experimentally derived gate-tunable junction transmission from the temperature dependence of the switching current. Due to the gate tunability of the junction, we can conclude that the observed half-integer Shapiro steps originated from the ballistic transport in the nanowire. The present study elucidated the relation between the junction CPR and the junction dynamics of the AC Josephson effect and may provide appropriate knowledge and methods for exploring the topological phenomena of the proximitized superconducting dynamics that is realized in superconductor-nanowire junctions.

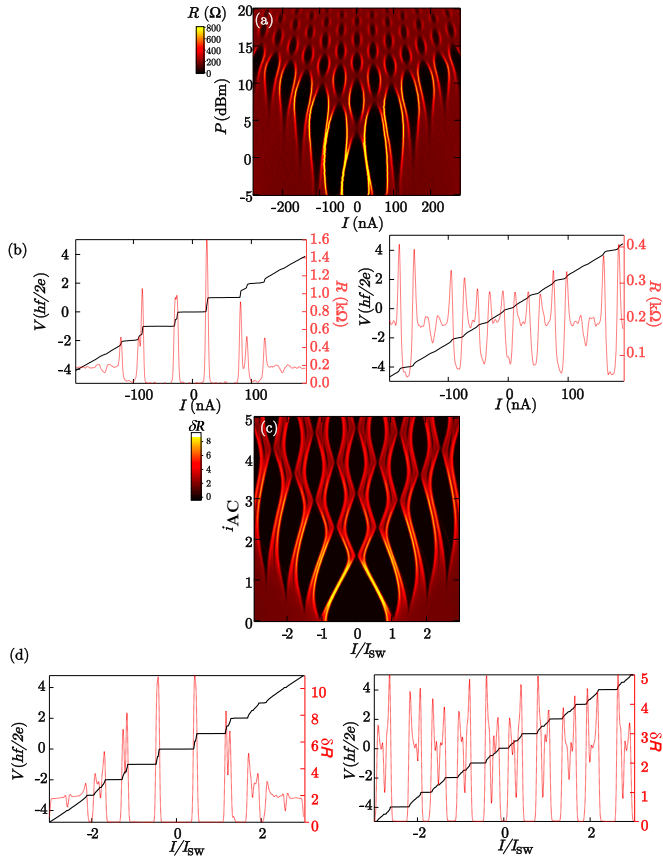


FIG. 5. (a) Plot of  $R$  as a function of  $I$  and  $P$  at  $f = 4.2$  GHz,  $V_g = 0$  V, and  $T = 50$  mK. (b) Observed Shapiro steps (black curves) at  $f = 4.2$  GHz,  $V_g = 0$  V, and  $P = 0$  dBm (left panel) and  $P = 15$  dBm (right panel). The red curves show  $R$  of the  $I$ - $V$  curve. (c) Simulated  $R$  as a function of  $I/I_{sw}$  and  $i_{AC}$  at  $\beta = 0.01$  and  $f' = 0.095$ . (d) Numerically simulated Shapiro steps at  $\beta = 0.01$ ,  $f' = 0.095$ , and  $i_{AC} = 2$  and  $5$ .

## ACKNOWLEDGMENTS

We thank S. Jeppesen for technical support to the material growth. This work was partially supported by a Grant-in-Aid for Scientific Research (B) (Grant No. JP18H01813), a Grant-in-Aid for Scientific Research (S) (Grant No. JP19H05610), the JSPS Program for Leading Graduate Schools (MERIT), the JSPS Research Fellowship for Young Scientists (Grants No. JP19J13867 and No. JP18J14172) from JSPS, JST PRESTO (Grant No. JPMJPR18L8), the Ministry of Science and Technology of China through the National Key Research and Development Program of China (Grants No. 2016YFA0300601 and No. 2017YFA0303304), the National Natural Science Foundation of China (Grants No. 91221202, No. 91421303, and No. 11874071), and the Swedish Research Council (VR).

## APPENDIX

### 1. Additional data of Shapiro steps

We executed the Shapiro step measurement with the microwave frequency  $f = 4.2$  GHz. We observed the half-integer steps at various  $P$ , not only at  $P = 6$  dBm [Fig. 2(a)].

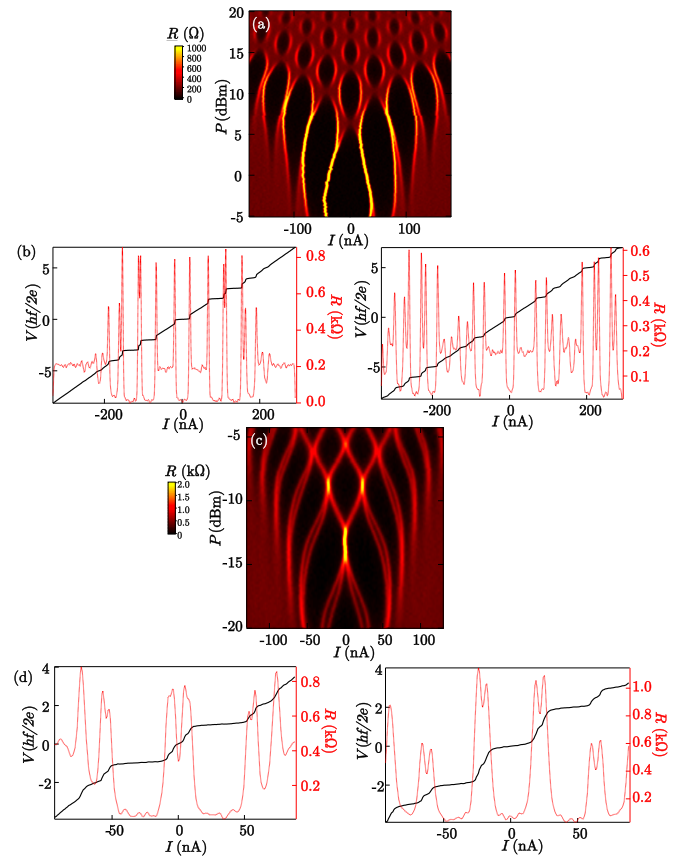


FIG. 6. Shapiro steps at other frequencies. (a) Plot of  $R$  as a function of  $I$  and  $P$  at  $f = 3.7$  GHz and  $V_g = 0$  V. (b) Shapiro steps (black curves) at  $f = 3.7$  GHz,  $V_g = 0$  V, and  $P = 10$  dBm (left panel) and  $P = 15$  dBm (right panel). The red curves show  $R$  of the  $I$ - $V$  curve. (c) Plot of  $R$  as a function of  $I$  and  $P$  at  $f = 1.8$  GHz and  $V_g = 0$  V. (d) Shapiro steps (black curves) at  $f = 1.8$  GHz,  $V_g = 0$  V, and  $P = -16$  dBm (left panel) and  $P = -10$  dBm (right panel). The red curves show  $R$  of the  $I$ - $V$  curve.

Figure 5(a) shows  $R$  as a function of  $I$  and  $P$ . The curves in Figs. 5(b) and 2(a) are taken from Fig. 5(a). The left and right panels of Fig. 5(b) were obtained at  $P = 0$  and  $15$  dBm. In the left panel, the half-integer steps appear at  $V = (\pm n/2)(hf/2e)$  ( $n = 1, 3$ ). In the  $P = 15$  dBm case, smeared half-integer steps are observed.

A calculated color plot of  $R$  as a function of  $I$  and  $P$  is shown in Fig. 5(c). The numerically calculated Shapiro steps at  $\beta = 0.01$  and  $f' = 0.095$  [see Eq. (2) for the parameters] are shown in Fig. 5(c). The curves in Fig. 5(d) are in qualitative agreement with the experimental data of Fig. 5(b). The left and right panels in Fig. 5(d) correspond to the line profiles at  $i_{AC} = 2$  and  $5$ , respectively. In our numerical calculation, one-third and two-third steps appear in addition to the half-integer steps. This reflects the third harmonic component of the short ballistic CPR.

### 2. Shapiro step measurement at other frequencies

The half-integer steps were observed with various  $f$ . Here we show our results with  $f = 3.7$  and  $1.8$  GHz. The curves in Fig. 6(b) represent line profiles at  $f = 3.7$  GHz in Fig. 6(a).

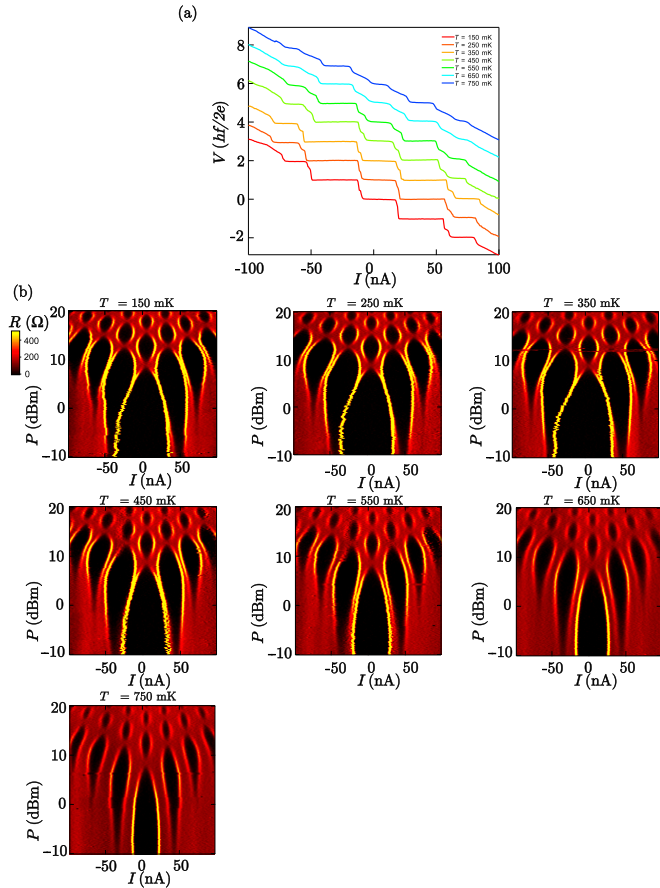


FIG. 7. (a) Temperature dependence of the Shapiro steps (offset clearly). These steps were measured at  $P = 6$  dBm and  $f = 4.2$  GHz. (b) Plot of  $R$  as a function of  $I$  and  $P$  at  $T = 150, 250, 350, 450, 550, 650,$  and  $750$  mK.

The left and right panels are obtained at  $P = 10$  and  $15$  dBm, respectively. On the other hand, the curves in Fig. 6(d) represent line profiles at  $f = 1.8$  GHz in Fig. 6(c). The left and right panels were acquired at  $P = -16$  and  $-10$  dBm. In all the  $I$ - $V$  curves, the half-integer steps are observed.

### 3. Temperature dependence of the half-integer steps

The Shapiro steps at  $f = 4.2$  GHz and  $P = 6$  dBm measured at  $T = 150, 250, 350, 450, 550, 650,$  and  $750$  mK are shown in Fig. 7(a). We note that  $P$  in this figure is different from that of Fig. 4(b). The y axis shows the data for 150 mK; the other data are incrementally shifted upward by  $hf/2e$ . As with the data shown in Fig. 4(b), the half-integer steps become vague and disappear as  $T$  increases; on the other hand, the integer steps remain. A color plot of  $R$  as a function of  $I$  and  $P$  at  $T = 150, 250, 350, 450, 550, 650,$  and  $750$  mK is shown in Fig. 7(b).

### 4. Temperature dependence of the integer step length

We introduced the normalized integer Shapiro step length as a ratio of length of the integer Shapiro steps at each temperature to that at  $T = 150$  mK. Normalized step length as a function of temperature is shown in Fig. 8. Figures 8(a),

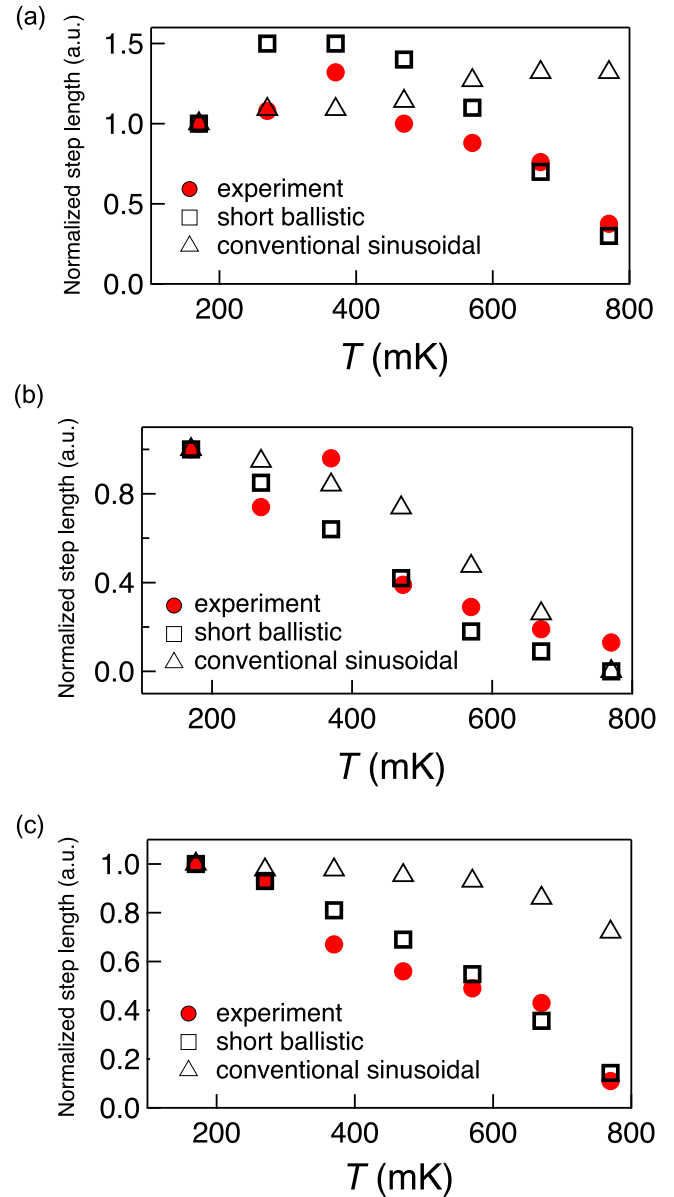


FIG. 8. Temperature dependence of normalized step length ratio at  $V = nhf/2e$  for (a)  $n = 0$ , (b)  $n = 1$ , and (c)  $n = 2$ . The close circles, open squares, and open triangles represent our experimental data, simulated results of the short ballistic CPR, and simulated results of the sinusoidal CPR, respectively.

8(b), and 8(c) represent the length of the steps with  $n = 0, 1,$  and  $2$ , respectively. The circles represent the experimental results at  $V_g = 0$  V. The squares indicate the numerical results using the RCSJ model with the CPR of the short ballistic Josephson junctions. In this calculation, we used  $\tau = 0.98$  and  $\beta = 0.008$ . The experimental results show good agreement with the numerical results. For comparison, we calculated the normalized step length with the sinusoidal CPR shown as the triangles. The results in the sinusoidal CPR case do not reproduce the experimental results. This supports our conclusion that the measured Josephson junction holds the skewed CPR and the estimated  $\tau$  is reasonable.

### 5. Capacitance estimation

The total capacitance  $C_{\text{total}}$  is represented as the sum of the geometric capacitance  $C$  and the intrinsic capacitance  $C_*$  [36]. The capacitance including the intrinsic capacitance changes

from 130 fF in the main text to 166 fF, resulting in the modified Stewart-McCumber parameter from 0.008 to 0.01. This modification causes no significant change in our numerical results. Therefore, we do not include this intrinsic capacitance term in our discussion.

- 
- [1] B. Joesphson, *Phys. Lett.* **1**, 251 (1962).
- [2] C. A. Hamilton, *Rev. Sci. Instrum.* **71**, 3611 (2000).
- [3] J. Koch, T. M. Yu, J. Gambetta, A. A. Houck, D. I. Schuster, J. Majer, A. Blais, M. H. Devoret, S. M. Girvin, and R. J. Schoelkopf, *Phys. Rev. A* **76**, 042319 (2007).
- [4] M. H. Devoret and R. J. Schoelkopf, *Science* **339**, 1169 (2013).
- [5] S. Shapiro, *Phys. Rev. Lett.* **11**, 80 (1963).
- [6] M. J. Renne and D. Polder, *Rev. Phys. Appl.* **9**, 25 (1974).
- [7] J. R. Waldram and P. H. Wu, *J. Low Temp. Phys.* **47**, 363 (1982).
- [8] A. H. Dayem and J. J. Wiegand, *Phys. Rev.* **155**, 419 (1967).
- [9] T. Klapwijk and T. Veenstra, *Phys. Lett. A* **47**, 351 (1974).
- [10] P. Dubos, H. Courtois, O. Buisson, and B. Pannetier, *Phys. Rev. Lett.* **87**, 206801 (2001).
- [11] F. Chiodi, M. Ferrier, S. Guéron, J. C. Cuevas, G. Montambaux, F. Fortuna, A. Kasumov, and H. Bouchiat, *Phys. Rev. B* **86**, 064510 (2012).
- [12] G.-H. Lee, S. Kim, S.-H. Jhi, and H.-J. Lee, *Nat. Commun.* **6**, 6181 (2015).
- [13] R. A. Snyder, C. J. Trimble, C. C. Rong, P. A. Folkes, P. J. Taylor, and J. R. Williams, *Phys. Rev. Lett.* **121**, 097701 (2018).
- [14] J. Basset, M. Kuzmanovic, P. Virtanen, T. T. Heikkilä, J. Esteve, J. Gabelli, C. Strunk, and M. Aprili, *Phys. Rev. Research* **1**, 032009(R) (2019).
- [15] P. E. Gregers-Hansen, M. T. Levinsen, and G. F. Pedersen, *J. Low Temp. Phys.* **7**, 99 (1972).
- [16] L. E. Hasselberg, M. T. Levinsen, and M. R. Samuelsen, *J. Low Temp. Phys.* **21**, 567 (1975).
- [17] A. Valizadeh, M. R. Kollahchi, and J. P. Straley, *J. Nonlinear Math. Phys.* **15**, 407 (2008).
- [18] H. Sellier, C. Baraduc, F. Lefloch, and R. Calemczuk, *Phys. Rev. Lett.* **92**, 257005 (2004).
- [19] S. M. Frolov, D. J. Van Harlingen, V. V. Bolginov, V. A. Oboznov, and V. V. Ryazanov, *Phys. Rev. B* **74**, 020503(R) (2006).
- [20] M. J. A. Stoutimore, A. N. Rossolenko, V. V. Bolginov, V. A. Oboznov, A. Y. Rusanov, D. S. Baranov, N. Pugach, S. M. Frolov, V. V. Ryazanov, and D. J. Van Harlingen, *Phys. Rev. Lett.* **121**, 177702 (2018).
- [21] L. P. Rokhinson, X. Liu, and J. K. Furdyna, *Nat. Phys.* **8**, 795 (2012).
- [22] J. Wiedenmann, E. Bocquillon, R. S. Deacon, S. Hartinger, O. Herrmann, T. M. Klapwijk, L. Maier, C. Ames, C. Brüne, C. Gould, A. Oiwa, K. Ishibashi, S. Tarucha, H. Buhmann, and L. W. Molenkamp, *Nat. Commun.* **7**, 10303 (2016).
- [23] E. Bocquillon, R. S. Deacon, J. Wiedenmann, P. Leubner, T. M. Klapwijk, C. Brüne, K. Ishibashi, H. Buhmann, and L. W. Molenkamp, *Nat. Nanotechnol.* **12**, 137 (2017).
- [24] C. Li, J. C. de Boer, B. de Ronde, S. V. Ramankutty, E. van Heumen, Y. Huang, A. de Visser, A. A. Golubov, M. S. Golden, and A. Brinkman, *Nat. Mater.* **17**, 875 (2018).
- [25] C. Nayak, S. H. Simon, A. Stern, M. Freedman, and S. Das Sarma, *Rev. Mod. Phys.* **80**, 1083 (2008).
- [26] J. Alicea, Y. Oreg, G. Refael, F. Von Oppen, and M. P. Fisher, *Nat. Phys.* **7**, 412 (2011).
- [27] S. D. Sarma, M. Freedman, and C. Nayak, *npj Quantum Inf.* **1**, 15001 (2015).
- [28] E. M. Spanton, M. Deng, S. Vaitiekėnas, P. Krogstrup, J. Nygård, C. M. Marcus, and K. A. Moler, *Nat. Phys.* **13**, 1177 (2017).
- [29] S. Hart, Z. Cui, G. Ménard, M. Deng, A. E. Antipov, R. M. Lutchyn, P. Krogstrup, C. M. Marcus, and K. A. Moler, *Phys. Rev. B* **100**, 064523 (2019).
- [30] S. Baba, S. Matsuo, H. Kamata, R. Deacon, A. Oiwa, K. Li, S. Jeppesen, L. Samuelson, H. Xu, and S. Tarucha, *Appl. Phys. Lett.* **111**, 233513 (2017).
- [31] S. Baba, C. Jünger, S. Matsuo, A. Baumgartner, Y. Sato, H. Kamata, K. Li, S. Jeppesen, L. Samuelson, H. Xu, C. Schönenberger, and S. Tarucha, *New J. Phys.* **20**, 063021 (2018).
- [32] H. Kamata, R. S. Deacon, S. Matsuo, K. Li, S. Jeppesen, L. Samuelson, H. Q. Xu, K. Ishibashi, and S. Tarucha, *Phys. Rev. B* **98**, 041302(R) (2018).
- [33] K. Ueda, S. Matsuo, H. Kamata, S. Baba, Y. Sato, Y. Takeshige, K. Li, S. Jeppesen, L. Samuelson, H. Xu, and S. Tarucha, *Sci. Adv.* **5**, eaaw2194 (2019).
- [34] W. Stewart, *Appl. Phys. Lett.* **12**, 277 (1968).
- [35] D. McCumber, *J. Appl. Phys.* **39**, 3113 (1968).
- [36] D. S. Antonenko and M. A. Skvortsov, *Phys. Rev. B* **92**, 214513 (2015).
- [37] K. Likharev, *Rev. Mod. Phys.* **51**, 101 (1979).
- [38] H. Courtois, M. Meschke, J. T. Peltonen, and J. P. Pekola, *Phys. Rev. Lett.* **101**, 067002 (2008).
- [39] M. Hurd, S. Datta, and P. F. Bagwell, *Phys. Rev. B* **54**, 6557 (1996).
- [40] I. O. Kulik and A. N. Omel'yanchuk, *Fizika Nizkikh Temperatur* **4**, 296 (1978).
- [41] W. Haberkorn, H. Knauer, and J. Richter, *Phys. Status Solidi A* **47**, K161 (1978).
- [42] C. W. J. Beenakker, in *Transport Phenomena in Mesoscopic Systems*, edited by H. Fukuyama and T. Ando, Springer Series in Solid-State Sciences Vol. 109 (Springer, Berlin, 1992), pp. 235–253.
- [43] A. Furusaki, H. Takayanagi, and M. Tsukada, *Phys. Rev. B* **45**, 10563 (1992).
- [44] M. F. Goffman, C. Urbina, H. Pothier, J. Nygård, C. M. Marcus, and P. Krogstrup, *New J. Phys.* **19**, 092002 (2017).
- [45] S. Hart, H. Ren, M. Kosowsky, G. Ben-Shach, P. Leubner, C. Brüne, H. Buhmann, L. W. Molenkamp, B. I. Halperin, and A. Yacoby, *Nat. Phys.* **13**, 87 (2016).

- [46] A. Murani, A. Kasumov, S. Sengupta, Y. A. Kasumov, V. T. Volkov, I. I. Khodos, F. Brisset, R. Delagrangé, A. Chepelianskii, R. Deblock, H. Bouchiat, and S. Guéron, *Nat. Commun.* **8**, 15941 (2017).
- [47] J. A. van Dam, Y. V. Nazarov, E. P. A. M. Bakkers, S. D. Franceschi, and L. P. Kouwenhoven, *Nature (London)* **442**, 667 (2006).
- [48] H. I. Jørgensen, T. Novotný, K. Grove-Rasmussen, K. Flensberg, and P. E. Lindelof, *Nano Lett.* **7**, 2441 (2007).
- [49] A. Eichler, R. Deblock, M. Weiss, C. Karrasch, V. Meden, C. Schönenberger, and H. Bouchiat, *Phys. Rev. B* **79**, 161407(R) (2009).
- [50] S. Li, N. Kang, P. Caroff, and H. Q. Xu, *Phys. Rev. B* **95**, 014515 (2017).